

Measurement of Coherent Production of π^\pm in Neutrino and Anti-Neutrino Beams on Carbon from E_ν of 1.5 to 20 GeV

A. Higuera,^{1,2} A. Mislivec,¹ L. Aliaga,^{3,4} O. Altinok,⁵ A. Bercellie,¹ M. Betancourt,⁶ A. Bodek,¹ A. Bravar,⁷ W.K. Brooks,⁸ H. Budd,¹ A. Butkevich,⁹ M.F. Carneiro,¹⁰ C.M. Castromonte,¹⁰ M.E. Christy,¹¹ J. Chvojka,¹ H. da Motta,¹⁰ J. Devan,³ S.A. Dytman,¹² G.A. Díaz,⁴ B. Eberly,^{12,*} J. Felix,² L. Fields,¹³ R. Fine,¹ G.A. Fiorentini,¹⁰ H. Gallagher,⁵ A. Gomez,¹ R. Gran,¹⁴ D.A. Harris,⁶ K. Hurtado,^{10,15} J. Kleykamp,¹ M. Kordosky,³ T. Le,¹⁶ E. Maher,¹⁷ S. Manly,¹ W.A. Mann,⁵ C.M. Marshall,¹ D.A. Martinez Caicedo,^{10,6} K.S. McFarland,^{1,6} C.L. McGivern,¹² A.M. McGowan,¹ B. Messerly,¹² J. Miller,⁸ J.G. Morfín,⁶ J. Mousseau,¹⁸ T. Muhlbeier,¹⁰ D. Naples,¹² J.K. Nelson,³ A. Norrick,³ J. Osta,⁶ J.L. Palomino,¹⁰ V. Paolone,¹² J. Park,¹ C.E. Patrick,¹³ G.N. Perdue,^{6,1} R.D. Ransome,¹⁶ H. Ray,¹⁸ L. Ren,¹² P.A. Rodrigues,¹ D. Ruterbories,¹ H. Schellman,¹³ D.W. Schmitz,^{19,6} F.D. Snider,⁶ C.J. Solano Salinas,¹⁵ N. Tagg,²⁰ B.G. Tice,^{16,†} E. Valencia,² T. Walton,¹¹ J. Wolcott,¹ M.Wospakrik,¹⁸ G. Zavala,² D. Zhang,³ and B.P.Ziemer²¹

(The MINERvA Collaboration)

¹University of Rochester, Rochester, New York 14627 USA

²Campus León y Campus Guanajuato, Universidad de Guanajuato, Lascruain de Retana No. 5, Colonia Centro. Guanajuato 36000, Guanajuato México.

³Department of Physics, College of William & Mary, Williamsburg, Virginia 23187, USA

⁴Sección Física, Departamento de Ciencias, Pontificia Universidad Católica del Perú, Apartado 1761, Lima, Perú

⁵Physics Department, Tufts University, Medford, Massachusetts 02155, USA

⁶Fermi National Accelerator Laboratory, Batavia, Illinois 60510, USA

⁷University of Geneva, 1211 Geneva 4, Switzerland

⁸Departamento de Física, Universidad Técnica Federico Santa María, Avenida España 1680 Casilla 110-V, Valparaíso, Chile

⁹Institute for Nuclear Research of the Russian Academy of Sciences, 117312 Moscow, Russia

¹⁰Centro Brasileiro de Pesquisas Físicas, Rua Dr. Xavier Sigaud 150, Urca, Rio de Janeiro, RJ, 22290-180, Brazil

¹¹Hampton University, Dept. of Physics, Hampton, VA 23668, USA

¹²Department of Physics and Astronomy, University of Pittsburgh, Pittsburgh, Pennsylvania 15260, USA

¹³Northwestern University, Evanston, Illinois 60208

¹⁴Department of Physics, University of Minnesota – Duluth, Duluth, Minnesota 55812, USA

¹⁵Universidad Nacional de Ingeniería, Apartado 31139, Lima, Perú

¹⁶Rutgers, The State University of New Jersey, Piscataway, New Jersey 08854, USA

¹⁷Massachusetts College of Liberal Arts, 375 Church Street, North Adams, MA 01247

¹⁸University of Florida, Department of Physics, Gainesville, FL 32611

¹⁹Enrico Fermi Institute, University of Chicago, Chicago, IL 60637 USA

²⁰Department of Physics, Otterbein University, 1 South Grove Street, Westerville, OH, 43081 USA

²¹Department of Physics and Astronomy, University of California, Irvine, Irvine, California 92697-4575, USA

(Dated: November 26, 2014)

Neutrino-induced coherent charged pion production on nuclei, $\bar{\nu}_\mu A \rightarrow \mu^\pm \pi^\mp A$ is a rare, inelastic interaction in which a small squared four-momentum $|t|$ is transferred to the recoil nucleus leaving it intact in the reaction. In the scintillator tracker of MINERvA, we remove events with evidence of particles from nuclear breakup and reconstruct $|t|$ from the final state pion and muon. We select low $|t|$ events to isolate a sample rich in coherent candidates. By selecting low $|t|$ events, we produce a model-independent measurement of the differential cross section for coherent scattering of neutrinos and anti-neutrinos on carbon. We find poor agreement with the predicted kinematics in neutrino generators used by current oscillation experiments.

PACS numbers: 13.15.+g,25.30.Pt

Coherent pion production from nuclei is an electroweak process described by the diagram in Fig. 1 in which a virtual pion scatters from a target nucleus that remains unchanged in its ground state after scattering. To achieve this coherence, the square of the four-momentum exchanged with the nucleus must be small, $|t| \lesssim \hbar^2/R^2$, where R is the radius of the nucleus, and the particle(s) exchanged can only carry vacuum quantum numbers.

Adler's theorem[1] provides a relationship between the coherent scattering cross section at $Q^2 \equiv -q^2 = 0$ and the pion-nucleus elastic cross section[2–4], which in the limit of $m_\mu, m_\pi \ll E_\nu$ is

$$\left. \frac{d^3\sigma_{coh}}{dQ^2 dy d|t|} \right|_{Q^2=0} = \frac{G_F^2}{2\pi^2} f_\pi^2 \frac{1-y}{y} \frac{d\sigma(\pi A \rightarrow \pi A)}{d|t|}, \quad (1)$$

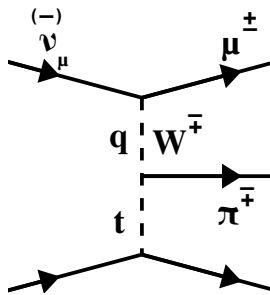


FIG. 1: Feynman diagram for coherent charged pion production

where y is E_π/E_ν and f_π is the pion decay constant. The πA elastic scattering cross section falls with increasing $|t| \sim e^{-|t|R^2/\hbar^2}$ [3, 4]. Models must be used to extrapolate to $Q^2 \neq 0$. The model most commonly used in neutrino event generators[5–7] is that of Rein and Sehgal[4], which assumes no vector current and extrapolates the axial-vector current using a multiplicative dipole form factor, $F_{dipole}^2(Q^2) = 1/(1 + Q^2/m_A^2)^2$, to modify Eq. 1. Other authors have proposed alternate extrapolations to $Q^2 \neq 0$ [8–11]. It is also necessary to parametrize the πA elastic scattering cross section, and generators have varied approaches[5–7]. At low energies, modifications to Eq. 1 due to finite masses become important, in particular $Q^2 \geq m_\mu^2 \frac{y}{1-y}$ and $|t| \geq \left(\frac{Q^2 + m_\pi^2}{2yE_\nu}\right)^2$ [12, 13]. An alternate approach for calculating the cross section at low neutrino energies is to relate it to low W (hadronic invariant mass) inclusive pion production[14–18].

Interest in coherent pion production has recently revived because of accelerator neutrino oscillation experiments[19–22] in which this reaction is a background to quasielastic neutrino-nucleon interactions when a π^0 or a π^\pm is mistaken for an e^\pm or proton, respectively. Recently, low energy experiments, K2K[23] and SciBooNE[24], did not observe coherent π^+ production at neutrino energies ~ 1 GeV at the level predicted by the Rein-Sehgal model[4] as then implemented in the NEUT[6] and NUANCE[7] event generators. There is strong experimental evidence for coherent π^0 production at these energies[25, 26].

In this letter, we identify a sample of coherent π^\pm candidates from neutrino and anti-neutrino beams on a scintillator (primarily CH) target by reconstructing the final state μ^\mp and π^\pm , allowing only minimal additional energy near the neutrino interaction vertex and requiring small $|t|$ as a signature of the coherent reaction. Non-coherent backgrounds are constrained with a sideband with high $|t|$. In contrast to other low energy measurements[23–28] which rely on selection in the pion kinematics or in Q^2 , this approach uses only model-independent characteristics of coherent pion production and therefore allows a measurement of the distribution of pion energies and angles in coherent reactions to test

the models.

The MINERvA experiment studies neutrinos produced in the NuMI beamline[29]. A beam of 120 GeV protons strike a graphite target, and charged mesons are focused by two magnetic horns into a 675 m helium-filled decay pipe. The horns focus positive (negative) mesons, resulting in a ν_μ ($\bar{\nu}_\mu$) enriched beam with a peak neutrino energy of 3.5 GeV. This analysis uses data taken between October 2009 and April 2012 with 3.05×10^{20} POT (protons on target) in ν_μ mode and 2.01×10^{20} POT in $\bar{\nu}_\mu$ mode.

The neutrino beam is simulated in a Geant4-based model[30, 31] constrained to reproduce hadron production measurements on carbon by the NA49 and MIPP experiments[32, 33]. Hadronic interactions not constrained by the NA49 or MIPP data are predicted using the FTFP hadron shower model¹. The uncertainty on the prediction of the neutrino flux is set by the precision in these hadron production measurements, uncertainties in the beam line focusing system and alignment[34], and comparisons between different hadron production models in regions not covered by the NA49 or MIPP data.

The MINERvA detector consists of a core of scintillator strips surrounded by electromagnetic and hadronic calorimeters on the sides and downstream end of the detector²[35]. The triangular 3.4×1.7 cm² strips are perpendicular to the z-axis³ and are arranged in hexagonal planes. Three plane orientations, 0° and $\pm 60^\circ$ rotations around the z-axis, enable reconstruction of the neutrino interaction point and the tracks of outgoing charged particles in three dimensions. The 3.0 ns timing resolution per plane allows separation of multiple interactions within a single beam spill. MINERvA is located 2 m upstream of the MINOS near detector, a magnetized iron spectrometer[20] which is used in this analysis to reconstruct the momentum and charge of μ^\pm . The MINERvA detector’s response is simulated by a tuned Geant4-based[30, 31] program. The energy scale of the detector is set by ensuring that both the photostatistics and the reconstructed energy deposited by momentum-analyzed through-going muons agree in data and simulation. The calorimetric constants used to reconstruct the energy of π^\pm showers and the corrections for passive material are determined from the simulation[35].

To estimate backgrounds, neutrino interactions are simulated using the GENIE 2.6.2 neutrino event generator[5]. For quasielastic interactions, the cross section is given by the Llewellyn Smith formalism[36]. Vector form factors come from fits to electron scat-

¹ FTFP shower model in Geant4 version 9.2 patch 03.

² The MINERvA scintillator tracking region is 95% CH and 5% other materials by weight.

³ The y-axis points along the zenith and the beam is directed downward by 58 mrad in the y-z plane.

tering data[37]; the axial form factor used is a dipole with an axial mass (M_A) of 0.99 GeV/c², consistent with deuterium measurements[38, 39], and sub-leading form factors are assumed from PCAC or exact G-parity symmetry[40]. The nuclear model is the relativistic Fermi gas (RFG) with a Fermi momentum of 221 MeV/c and an extension to higher nucleon momenta due to short-range correlations[41, 42]. Inelastic, low W reactions are simulated with a tuned model of discrete baryon resonance production[43], and the transition to deep inelastic scattering is simulated using the Bodek-Yang model[44]. Hadronization at higher energies is simulated with the AGKY model[45] which is based on the gradual transition from KNO scaling to the LUND string model of PYTHIA with increasing W . Final state interactions, in which hadrons interact within the target nucleus, are modeled using the INTRANUKE package[5]. Uncertainties in the parameters of these models are assigned based on either measurement uncertainties from data or to cover differences between external datasets and GENIE's model.

The MINERvA detector[35] records the energy and time of energy depositions (hits) in each scintillator strip. Hits are first grouped in time and then clusters of energy are formed by spatially grouping the hits in each scintillator plane. Clusters with energy > 1 MeV are then matched among the three views to create a track. The μ^\pm candidate is a track that exits the back of MINERvA matching a track of the expected charge entering the front of MINOS. The most upstream cluster on the muon track is taken to be the interaction vertex. The resolution of each track cluster is 2.7 mm and the angular resolution of the muon track is better than 10 mrad in each view. The reconstruction of the muon in the MINOS spectrometer gives a typical muon momentum resolution of 11%. Event pile-up causes a decrease in the muon track reconstruction efficiency which was studied in both MINERvA and MINOS by projecting tracks found in one detector to the other and measuring the misreconstruction rate. This results in a -7.8% (-4.6%) correction to the simulated efficiency for muons below (above) 3 GeV/c.

The interaction vertex is restricted to be within the central 108 planes of the scintillator tracking region and no closer than 22 cm to any edge of the planes. These requirements define a region with a mass of 5.47 metric tons. In the anti-neutrino exposure, 45% of the POT were taken during the construction of the MINERvA detector and therefore only used a fraction of the downstream tracker, with a fiducial volume of 56 planes and a mass of 2.84 metric tons.

Charged π^\pm reconstruction requires a second track originating from the vertex. The angular resolution on this shorter track has a narrow central distribution with a full width at half maximum of 17 mrad; however the distribution has long tails due to pion scattering in the scintillator and has an RMS resolution of 160 mrad in each

view. For the neutrino beam, in which CCQE events with a proton misidentified as a π^+ are a background, dE/dx along the track is required to be inconsistent with that expected from a proton ranging out in the detector. This cut removes 64% of protons in the simulation while retaining 95% of π^\pm . The energy of the charged pion is reconstructed calorimetrically with a fractional resolution of $18\%+8\%/\sqrt{E_\pi/\text{GeV}}$, and it is this resolution that dominates the experimental resolution on $|t|$. From the measured muon and pion energies and directions,

$$|t| = \left| (p_\nu - p_\mu - p_\pi)^2 \right| \approx \left(\sum_{i=\mu,\pi} E_i - p_{i,L} \right)^2 + \left| \sum_{i=\mu,\pi} \vec{p}_{i,T} \right|^2, \quad (2)$$

where the approximation made is that zero energy is transferred to the recoil nucleus and where \vec{p}_T and p_L are the transverse and longitudinal momenta with respect to the known neutrino beam direction.

By definition, a coherent reaction produces a μ^\mp , a π^\pm , and nothing else originating from the interaction vertex. Vertex energy is defined as all energy deposited within five planes of the plane in which the neutrino interacts in strips within 20 cm of the interaction vertex. Energy deposited on the muon and pion tracks is corrected for path length in the bars. For coherent events, this results in a vertex energy of 50 MeV with an RMS spread of 10 MeV due to fluctuations in energy deposited by the muon and pion. Background processes typically leave significantly more energy in this region, and this analysis requires the reconstructed vertex energy to be between 30 and 70 MeV. This requirement removes 85(86)% of the predicted background in the $\nu_\mu(\bar{\nu}_\mu)$ measurement and keeps 87.0(86.7)% of the coherent pion events.

As shown in Fig. 2 (top), after the vertex energy requirement, the simulation exceeds the background at high $|t|$. The incoherent background components are divided into categories based on W , and scale factors for the background are estimated by fits to the distributions of π^\pm energies for events with $0.2 < |t| < 0.6$ (GeV/c)². As shown in Table I the fit reduces the predicted background, particularly at low W . The reconstructed $|t|$ distribution after background tuning is shown in Fig. 2 (bottom), and a significant excess of low $|t|$ events over the background-only prediction is observed. The scaled background is then subtracted from the events with $|t| < 0.125$ (GeV/c)² to measure the rate of coherent events in the data. There are 1628 and 770 coherent candidates after background subtraction in the neutrino and anti-neutrino samples respectively.

The cross section is determined by $\sigma = N_{\text{coh}}/\Phi N_{12C}$, where Φ is the total flux of neutrinos incident on the detector. Our scintillator has free protons in numbers equal to the ¹²C nuclei. GENIE does not simulate diffractive production of pions from the free protons which might

Source of Background	ν_μ	$\bar{\nu}_\mu$
Charged Current Quasielastic	0.7 ± 0.3	1 (fixed)
Non-quasielastic, $W < 1.4$ GeV	0.6 ± 0.3	0.7 ± 0.1
$1.4 < W < 2.0$ GeV	0.7 ± 0.1	0.6 ± 0.1
$W > 2.0$ GeV	1.1 ± 0.1	1.9 ± 0.3

TABLE I: Scale factors and their statistical uncertainties determined for different background sources, grouped by hadronic invariant mass, W , from the high $|t|$ sidebands

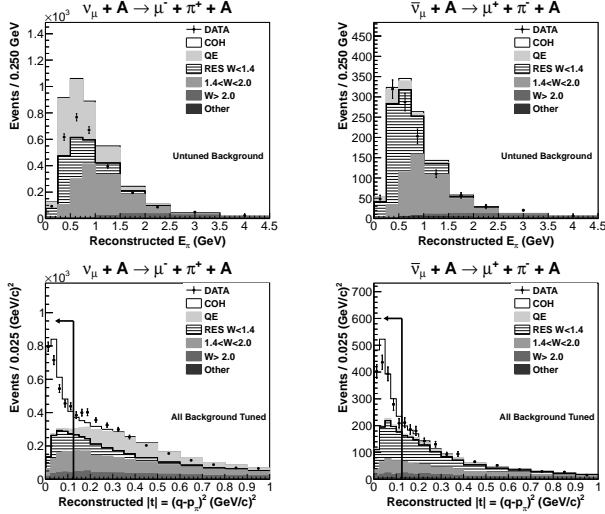


FIG. 2: (Top) pion energy distribution for events in the $0.2 < |t| < 0.6$ (GeV/c)² sideband, ν_μ (left) and $\bar{\nu}_\mu$ (right) beams and (bottom) reconstructed $|t|$ after background tuning using the sideband. The signal distribution in $|t|$ peaks near zero with its shape dominated by detector resolution.

also produce events at low $|t|$. There is no microphysical calculation of this process at our energies. An inclusive calculation of $\nu p \rightarrow \mu^\pm \pi^\mp p$ based on πA elastic scattering data and the Adler relation[1, 46], shows a modest low $|t|$ enhancement not seen in GENIE which falls exponentially with $|t|$. This difference does not identify diffractive events, but instead includes all low $|t|$ enhancements in scattering from protons that might be in this calculation. Moreover, most events with $|t| > 0.05$ GeV² would not pass our vertex energy requirement because of the recoiling proton's ionization. We estimate the acceptance of these low $|t|$ events to be $\approx 20\%$ of the acceptance for coherent events on carbon. Based this low $|t|$ enhancement and our acceptance, the event rate in our data would be equivalent to 7%(4%) of the GENIE prediction for the coherent cross-section on ¹²C for neutrinos(anti-neutrinos). We do not correct our result for this possible enhancement.

We measure flux-averaged⁴ cross sections of $(3.49 \pm$

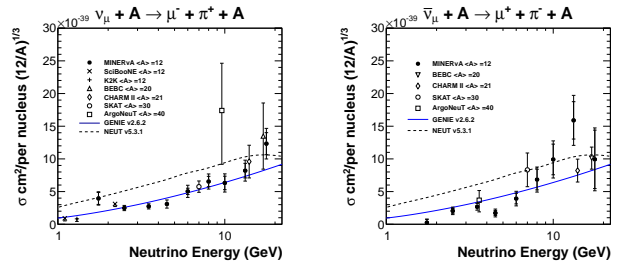


FIG. 3: $\sigma(E_\nu)$ for neutrino (left) and anti-neutrino (right) coherent π^\pm production. The inner error bars in the cross section represent statistical uncertainties and the outer the total uncertainties; the cross section is tabulated in the Appendix. Results from other measurements[23, 24, 28, 49–52] are scaled to carbon using the predicted $A^{1/3}$ dependence of the Rein-Sehgal model[4].

$E_{\nu(\bar{\nu})}$ (GeV)	I	II	III	IV	V	Total
1.5 – 2.0	0.101	0.041	0.031	0.017	0.002	0.115
2.0 – 3.0	0.108	0.058	0.040	0.034	0.020	0.135
3.0 – 4.0	0.099	0.053	0.041	0.037	0.027	0.127
4.0 – 5.0	0.163	0.046	0.040	0.038	0.029	0.180
ν 5.0 – 7.0	0.146	0.031	0.034	0.034	0.023	0.159
7.0 – 9.0	0.118	0.027	0.034	0.026	0.016	0.129
9.0 – 11.0	0.132	0.034	0.044	0.029	0.019	0.147
11.0 – 15.0	0.132	0.022	0.034	0.021	0.014	0.140
15.0 – 20.0	0.128	0.015	0.022	0.013	0.009	0.132
1.5 – 2.0	0.216	0.497	0.309	0.308	0.111	0.704
2.0 – 3.0	0.135	0.144	0.075	0.027	0.030	0.215
3.0 – 4.0	0.100	0.095	0.065	0.021	0.026	0.156
4.0 – 5.0	0.191	0.138	0.105	0.036	0.048	0.265
$\bar{\nu}$ 5.0 – 7.0	0.164	0.065	0.073	0.025	0.028	0.194
7.0 – 9.0	0.140	0.043	0.056	0.017	0.019	0.158
9.0 – 11.0	0.148	0.038	0.048	0.014	0.015	0.161
11.0 – 15.0	0.157	0.016	0.024	0.008	0.006	0.160
15.0 – 20.0	0.154	0.052	0.066	0.017	0.024	0.178

TABLE II: Fractional systematic uncertainties on $\sigma(E_\nu)$ and $\sigma(E_{\bar{\nu}})$ associated with Flux (I), neutrino interaction models (II), detector simulation (III), vertex energy (IV), and (V) sideband model. The final column shows the total systematic uncertainty due to all sources.

$0.11(\text{stat}) \pm 0.37(\text{flux}) \pm 0.20(\text{other sys.}) \times 10^{-39}$ and $(2.65 \pm 0.15(\text{stat}) \pm 0.31(\text{flux}) \pm 0.30(\text{other sys.})) \times 10^{-39}$ cm² per ¹²C nucleus in the neutrino and anti-neutrino beams respectively. In cross-sections as a function of E_ν , E_π and θ_π , the effect of detector resolution is accounted for by using iterative Bayesian unfolding[47, 48]. Figure 3 shows the measured cross sections as a function of E_ν compared with previous measurements for $E_\nu < 20$ GeV and with the NEUT[6] and GENIE[5] implementations⁵ of Rein and Sehgal[4] with lepton mass corrections[12].

⁴ The fluxes of neutrinos and anti-neutrinos in this analysis are given in the Appendix.

⁵ The pion-nucleus elastic cross section correction of GENIE 2.8.0 was implemented in the simulation.

The main sources of systematic uncertainty on the cross sections are the flux, the background interaction model, pion interactions in the detector, muon reconstruction, muon and hadron energy scale, vertex energy, and the model used in the sideband constraint for the background. These systematic uncertainties are shown in Table II. The uncertainty of hadron interactions in the detector as predicted by Geant4 on tracking and energy measurements is evaluated by varying the pion and proton total inelastic cross sections by $\pm 10\%$ and the neutron mean free path as a function of kinematic energy by 10–25% to span differences between Geant4 and hadron scattering data[53–64].

For muons reconstructed by range in MINOS, the muon energy scale uncertainty is dominated by energy loss uncertainties, and we compared range and curvature measurements to evaluate uncertainties on reconstruction of muons by curvature in the MINOS magnetic field. Uncertainties in the hadron energy reconstruction result from uncertainties in the energy scale set by muon energy deposition, material composition and dimensions, saturation of ionization in the scintillator, and photosensor cross talk and non-linearity. Comparisons with the test beam[35] limit the energy scale uncertainty for pions (protons) to 5% (3%). The target mass is uncertain to 1.4%.

Uncertainties in predictions for the non-coherent background from the GENIE generator are evaluated by varying the underlying model tuning parameters according to their uncertainties[5]. The most important parameters are the normalization and axial form factor for baryon resonance production. MINERvA’s measurements of the CCQE process[65, 66] show that GENIE does not model the energetic final state proton multiplicity well, which in turn means a mismodeling of the vertex energy. The resulting uncertainty is estimated by turning on and off the addition of energy deposited by a 20–225 MeV final state proton to the vertex energy of 25% of background events with a target neutron. Finally, after tuning the background we find remaining disagreement in the sideband θ_π distribution. This disagreement is corrected and the size of the correction is taken as a systematic uncertainty. The effects of these model variations are reduced by sideband tuning of the background.

Figure 4 compares the flux-averaged differential cross sections as a function of pion energy and angle against the Rein-Sehgal model[4] as implemented in GENIE[5, 12] and NEUT[6]. Disagreement at high θ_π is evident in both GENIE and NEUT. In GENIE, whose behavior is more similar to the data, the model predicts $\sim 15\%$ of the cross section with $\theta_\pi > 45^\circ$ but there is no evidence for such events in the data.

In conclusion, the coherent production of pions on carbon nuclei for both neutrino and anti-neutrino beams is precisely measured by isolating a sample with no visible nuclear breakup and low $|t|$ transferred to the nucleus.

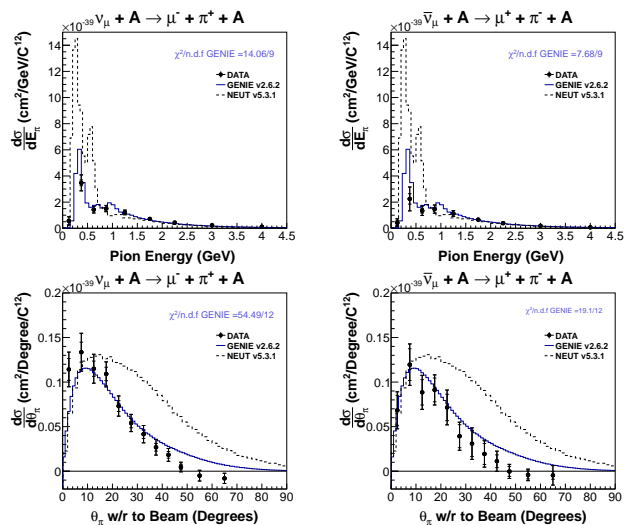


FIG. 4: $d\sigma/dE_\pi$ (top) and $d\sigma/d\theta_\pi$ (bottom) for ν_μ (left) and $\bar{\nu}_\mu$ (right) with error bars as in Fig. 3 compared against predicted cross-sections from GENIE[5] and NEUT[6]. These cross sections are tabulated in the Appendix.

This allows a study of produced pion kinematics independent of the details of the signal model. The cross sections of the neutrino and anti-neutrino coherent pion production are similar, indicating that the reaction is likely to be primarily an axial vector process. The discrepancies observed at neutrino energies relevant for the T2K oscillation experiment[21] suggest that these data should be used to revise the predictions of neutrino interaction models used in future measurements.

This work was supported by the Fermi National Accelerator Laboratory under US Department of Energy contract No. DE-AC02-07CH11359 which included the MINERvA construction project. Construction support was also granted by the United States National Science Foundation under Grant PHY-0619727 and by the University of Rochester. Support for participating scientists was provided by NSF and DOE (USA) by CAPES and CNPq (Brazil), by CoNaCyT (Mexico), by CONICYT (Chile), by CONCYTEC, DGI-PUCP and IDI/IGI-UNI (Peru), by Latin American Center for Physics (CLAF) and by RAS and the Russian Ministry of Education and Science (Russia). We thank the MINOS Collaboration for use of its near detector data. Finally, we thank the staff of Fermilab for support of the beamline and the detector.

* now at SLAC National Accelerator Laboratory, Stanford, California 94309 USA

† now at Argonne National Laboratory, Argonne, IL 60439, USA

[1] S. L. Adler, Phys.Rev. **135**, B963 (1964).

- [2] C. Piketty and L. Stodolsky, Nucl.Phys. **B15**, 571 (1970).
- [3] K. Lackner, Nucl.Phys. **B153**, 526 (1979).
- [4] D. Rein and L. M. Sehgal, Nucl.Phys. **B223**, 29 (1983).
- [5] C. Andreopoulos, A. Bell, D. Bhattacharya, F. Cavanna, J. Dobson, S. Dytman, H. Gallagher, P. Guzowski, R. Hatcher, P. Kehayias, A. Meregaglia, D. Naples, G. Pearce, A. Rubbia, M. Whalley, and T. Yang, Nuclear Instruments and Methods in Physics Research Section A: Accelerators, Spectrometers, Detectors and Associated Equipment **614**, 87 (2010), Program version 2.6.2 used here.
- [6] Y. Hayato, Acta Phys.Polon. **B40**, 2477 (2009).
- [7] D. Casper, Nucl.Phys.Proc.Suppl. **112**, 161 (2002), arXiv:hep-ph/0208030 [hep-ph] .
- [8] S. Gershtein, Y. Y. Komachenko, and M. Y. a. Khlopov, Sov.J.Nucl.Phys. **32**, 861 (1980).
- [9] A. Belkov and B. Kopeliovich, Sov.J.Nucl.Phys. **46**, 499 (1987).
- [10] C. Berger and L. Sehgal, Phys.Rev. **D79**, 053003 (2009), arXiv:0812.2653 [hep-ph] .
- [11] E. Paschos and D. Schalla, Phys.Rev. **D80**, 033005 (2009), arXiv:0903.0451 [hep-ph] .
- [12] D. Rein and L. Sehgal, Phys.Lett. **B657**, 207 (2007), arXiv:hep-ph/0606185 [hep-ph] .
- [13] A. Higuera and E. Paschos, Eur.Phys.J.Plus **129**, 43 (2014), arXiv:1311.5149 [hep-ph] .
- [14] S. Singh, M. Sajjad Athar, and S. Ahmad, Phys.Rev.Lett. **96**, 241801 (2006).
- [15] L. Alvarez-Ruso, L. Geng, S. Hirenzaki, and M. Vicente Vacas, Phys.Rev. **C75**, 055501 (2007), arXiv:nucl-th/0701098 [nucl-th] .
- [16] J. Amaro, E. Hernandez, J. Nieves, and M. Valverde, Phys.Rev. **D79**, 013002 (2009), arXiv:0811.1421 [hep-ph] .
- [17] T. Leitner, U. Mosel, and S. Winkelmann, Phys.Rev. **C79**, 057601 (2009), arXiv:0901.2837 [nucl-th] .
- [18] E. Hernandez, J. Nieves, and M. Vicente-Vacas, Phys.Rev. **D80**, 013003 (2009), arXiv:0903.5285 [hep-ph] .
- [19] Y. Oyama (K2K collaboration), (1998), arXiv:hep-ex/9803014 [hep-ex] .
- [20] D. G. Michael *et al.* (MINOS Collaboration), Nucl.Instrum.Meth. **A596**, 190 (2008), arXiv:0805.3170 [physics.ins-det] .
- [21] K. Abe *et al.* (T2K Collaboration), Nucl.Instrum.Meth. **A659**, 106 (2011), arXiv:1106.1238 [physics.ins-det] .
- [22] D. S. Ayres *et al.* (NOvA Collaboration), (2004), arXiv:hep-ex/0503053 [hep-ex] .
- [23] M. Hasegawa *et al.* (K2K Collaboration), Phys.Rev.Lett. **95**, 252301 (2005), arXiv:hep-ex/0506008 [hep-ex] .
- [24] K. Hiraide *et al.* (SciBooNE Collaboration), Phys.Rev. **D78**, 112004 (2008), arXiv:0811.0369 [hep-ex] .
- [25] A. Aguilar-Arevalo *et al.* (MiniBooNE Collaboration), Phys.Lett. **B664**, 41 (2008), arXiv:0803.3423 [hep-ex] .
- [26] Y. Kurimoto *et al.* (SciBooNE Collaboration), Phys.Rev. **D81**, 111102 (2010), arXiv:1005.0059 [hep-ex] .
- [27] T. Kikawa, “T2k on-axis coherent pion production,” (2014), NuINT14, 9th International Workshop on Neutrino-Nucleus Interactions in the Few GeV Region.
- [28] R. Acciarri *et al.* (ArgoNeuT Collaboration), (2014), arXiv:1408.0598 [hep-ex] .
- [29] K. Anderson, B. Bernstein, D. Boehnlein, K. R. Bourkland, S. Childress, *et al.*, *The NuMI Facility Technical Design Report*, FERMILAB-DESIGN-1998-01 (1998).
- [30] S. Agostinelli *et al.*, Nuclear Instruments and Methods in Physics Research Section A: Accelerators, Spectrometers, Detectors and Associated Equipment **506**, 250 (2003).
- [31] J. Allison *et al.*, Nuclear Science, IEEE Transactions on **53**, 270 (2006).
- [32] C. Alt *et al.* (NA49 Collaboration), Eur.Phys.J. **C49**, 897 (2007), arXiv:hep-ex/0606028 [hep-ex] .
- [33] A. V. Lebedev, *Ratio of pion kaon production in proton carbon interactions*, Ph.D. thesis, Harvard University (2007).
- [34] Z. Pavlovic, *Observation of Disappearance of Muon Neutrinos in the NuMI Beam*, Ph.D. thesis, University of Texas (2008).
- [35] L. Aliaga *et al.* (MINERvA Collaboration), Nucl.Instrum.Meth. **A743**, 130 (2014), arXiv:1305.5199 [physics.ins-det] .
- [36] C. H. Llewellyn Smith, Phys.Rept. **3**, 261 (1972).
- [37] R. Bradford, A. Bodek, H. S. Budd, and J. Arrington, Nucl.Phys.Proc.Suppl. **159**, 127 (2006), arXiv:hep-ex/0602017 [hep-ex] .
- [38] A. Bodek, S. Avvakumov, R. Bradford, and H. S. Budd, J.Phys.Conf.Ser. **110**, 082004 (2008), arXiv:0709.3538 [hep-ex] .
- [39] K. S. Kuzmin, V. V. Lyubushkin, and V. A. Naumov, Eur.Phys.J. **C54**, 517 (2008), arXiv:0712.4384 [hep-ph] .
- [40] M. Day and K. S. McFarland, Phys.Rev. **D86**, 053003 (2012), arXiv:1206.6745 [hep-ph] .
- [41] A. Bodek and J. L. Ritchie, Phys.Rev. **D23**, 1070 (1981).
- [42] A. Bodek and J. L. Ritchie, Phys.Rev. **D24**, 1400 (1981).
- [43] D. Rein and L. M. Sehgal, Annals Phys. **133**, 79 (1981).
- [44] A. Bodek, I. Park, and U.-K. Yang, Nucl.Phys.Proc.Suppl. **139**, 113 (2005), arXiv:hep-ph/0411202 [hep-ph] .
- [45] T. Yang, C. Andreopoulos, H. Gallagher, K. Hoffmann, and P. Kehayias, Eur.Phys.J. **C63**, 1 (2009), arXiv:0904.4043 [hep-ph] .
- [46] B. Z. Kopeliovich, “NP: Neutrinoproduction of pions off nuclei,” private communication, <http://www.fis.utfsm.cl/np/>.
- [47] G. D’Agostini, Nucl.Instrum.Meth. **A362**, 487 (1995).
- [48] T. Adye, , 313 (2011), arXiv:1105.1160 [physics.data-an] .
- [49] H. Grabosch *et al.* (SKAT Collaboration), Z.Phys. **C31**, 203 (1986).
- [50] P. Marage *et al.* (BEBC WA59 COLLABORATION), Z.Phys. **C31**, 191 (1986).
- [51] P. Allport *et al.* (BEBC WA59 Collaboration), Z.Phys. **C43**, 523 (1989).
- [52] P. Vilain *et al.* (CHARM-II Collaboration), Phys.Lett. **B313**, 267 (1993).
- [53] D. Ashery, I. Navon, G. Azuelos, H. Walter, H. Pfeiffer, and F. Schlepütz, Phys. Rev. C **23**, 2173 (1981).
- [54] B. Allardyce, C. Batty, D. Baugh, E. Friedman, G. Heymann, *et al.*, Nucl. Phys. **A209**, 1 (1973).
- [55] A. Saunders, S. Hoeibraten, J. Kraushaar, B. Kriss, R. Peterson, *et al.*, Phys. Rev. C **53**, 1745 (1996).
- [56] T. Lee and R. Redwine, Ann. Rev. Nucl. Part. Sci. **52**, 23 (2002).
- [57] W. P. Abfalterer, F. B. Bateman, F. S. Dietrich, R. W. Finlay, R. C. Haight, *et al.*, Phys.Rev. **C63**, 044608 (2001).
- [58] W. Schimmerling, T. J. Devlin, W. W. Johnson, K. G. Vosburgh, and R. E. Mischke, Phys.Rev. **C7**, 248 (1973).
- [59] R. G. P. Voss and R. Wilson, Proc.Roy.Soc. **A236**, 41

- (1956).
- [60] I. Slypen, V. Corcalciuc, and J. P. Meulders, *Phys.Rev.* **C51**, 1303 (1995).
 - [61] J. Franz, P. Koncz, E. Rossle, C. Sauerwein, H. Schmitt, *et al.*, *Nucl.Phys.* **A510**, 774 (1990).
 - [62] U. Tippawan, S. Pomp, J. Blomgren, S. Dangtip, C. Gustavsson, *et al.*, *Phys.Rev.* **C79**, 064611 (2009), arXiv:0812.0701 [nucl-ex] .
 - [63] R. Bevilacqua, S. Pomp, M. Hayashi, A. Hjalmarrsson, U. Tippawan, *et al.*, (2013), arXiv:1303.4637 [nucl-ex] .
 - [64] C. I. Zanelli, P. P. Urone, J. L. Romero, F. P. Brady, M. L. Johnson, *et al.*, *Phys.Rev.* **C23**, 1015 (1981).
 - [65] L. Fields, J. Chvojka, *et al.* (MINERvA Collaboration), *Phys.Rev.Lett.* **111**, 022501 (2013), arXiv:1305.2234 [hep-ex] .
 - [66] G. Fiorentini, D. Schmitz, *et al.* (MINERvA Collaboration), *Phys.Rev.Lett.* **111**, 022502 (2013), arXiv:1305.2243 [hep-ex] .

Appendix: Supplementary Material

E_π (GeV)	$d\sigma/dE_\pi$ ($cm^2/GeV/C^{12}$) $\times 10^{-39}$	$d\sigma/dE_\pi$ ($cm^2/GeV/C^{12}$) $\times 10^{-39}$
	neutrinos	antineutrinos
0 - 0.25	0.567 \pm 0.116 \pm 0.288	0.423 \pm 0.146 \pm 0.238
0.25 - 0.5	3.473 \pm 0.223 \pm 0.568	2.245 \pm 0.313 \pm 0.820
0.5 - 0.75	1.426 \pm 0.105 \pm 0.234	1.342 \pm 0.142 \pm 0.315
0.75 - 1.0	1.508 \pm 0.096 \pm 0.222	1.467 \pm 0.127 \pm 0.272
1.0 - 1.5	1.213 \pm 0.078 \pm 0.161	1.129 \pm 0.094 \pm 0.182
1.5 - 2.0	0.714 \pm 0.061 \pm 0.094	0.659 \pm 0.073 \pm 0.110
2.0 - 2.5	0.429 \pm 0.047 \pm 0.060	0.393 \pm 0.059 \pm 0.074
2.5 - 3.5	0.227 \pm 0.030 \pm 0.034	0.182 \pm 0.035 \pm 0.045
3.5 - 4	0.116 \pm 0.019 \pm 0.020	0.073 \pm 0.017 \pm 0.020

TABLE III: The measurement of the differential cross section as a function of pion energy, $d\sigma/dE_\pi$, with statistical and systematic uncertainties

θ_π (Degrees)	$d\sigma/d\theta_\pi$ ($cm^2/Degree/C^{12}$) $\times 10^{-39}$	$d\sigma/d\theta_\pi$ ($cm^2/Degree/C^{12}$) $\times 10^{-39}$
	neutrinos	antineutrinos
0 - 5	0.114 \pm 0.012 \pm 0.015	0.068 \pm 0.014 \pm 0.012
5 - 10	0.133 \pm 0.011 \pm 0.018	0.120 \pm 0.015 \pm 0.015
10 - 15	0.115 \pm 0.009 \pm 0.014	0.088 \pm 0.012 \pm 0.013
15 - 20	0.109 \pm 0.008 \pm 0.011	0.091 \pm 0.011 \pm 0.010
20 - 25	0.073 \pm 0.006 \pm 0.010	0.072 \pm 0.013 \pm 0.013
25 - 30	0.054 \pm 0.005 \pm 0.008	0.039 \pm 0.012 \pm 0.009
30 - 35	0.042 \pm 0.005 \pm 0.008	0.031 \pm 0.013 \pm 0.010
35 - 40	0.027 \pm 0.004 \pm 0.008	0.019 \pm 0.011 \pm 0.009
40 - 45	0.018 \pm 0.004 \pm 0.006	0.011 \pm 0.006 \pm 0.009
45 - 50	0.005 \pm 0.003 \pm 0.004	-0.000 \pm 0.004 \pm 0.006
50 - 60	-0.005 \pm 0.002 \pm 0.006	-0.004 \pm 0.004 \pm 0.005
60 - 70	-0.008 \pm 0.002 \pm 0.005	-0.005 \pm 0.003 \pm 0.010

TABLE IV: The measurement of the differential cross section as a function of pion angle, $d\sigma/d\theta_\pi$, with statistical and systematic uncertainties

E_ν (GeV)	σ (cm^2/C^{12}) $\times 10^{-39}$	σ (cm^2/C^{12}) $\times 10^{-39}$
	neutrinos	antineutrinos
1.5 - 2.0	3.952 \pm 0.914 \pm 0.454	0.254 \pm 0.494 \pm 0.179
2.0 - 3.0	2.485 \pm 0.214 \pm 0.335	2.049 \pm 0.290 \pm 0.440
3.0 - 4.0	2.736 \pm 0.183 \pm 0.349	2.673 \pm 0.243 \pm 0.417
4.0 - 5.0	3.096 \pm 0.276 \pm 0.559	1.725 \pm 0.311 \pm 0.457
5.0 - 7.0	5.037 \pm 0.478 \pm 0.798	3.928 \pm 0.666 \pm 0.763
7.0 - 9.0	6.540 \pm 0.791 \pm 0.844	6.840 \pm 1.294 \pm 1.084
9.0 - 11.0	6.321 \pm 1.033 \pm 0.932	9.917 \pm 1.863 \pm 1.601
11.0 - 15.0	8.205 \pm 1.115 \pm 1.149	15.896 \pm 2.245 \pm 2.538
15.0 - 20.0	12.330 \pm 1.686 \pm 1.622	9.931 \pm 3.477 \pm 1.768

TABLE V: The measurement of the cross section as a function of E_ν and statistical and systematic uncertainties

E_ν (GeV)	1.5 - 2.0	2.0 - 3.0	3.0 - 4.0	4.0 - 5.0	5.0 - 7.0	7.0 - 9.0	9.0 - 11.0	11.0 - 15.0	15.0 - 20.0
$(\nu/cm^2/POT/\times 10^{-8})$	0.291	0.865	0.906	0.375	0.206	0.100	0.0664	0.0871	0.0404
$(\bar{\nu}/cm^2/POT/\times 10^{-8})$	0.265	0.762	0.754	0.293	0.140	0.0556	0.0329	0.0391	0.0154

TABLE VI: The predicted neutrino and anti-neutrino beam fluxes for the data included in this analysis

$E_\pi(GeV)$	0 - 0.25	0.25 - 0.5	0.5 - 0.75	0.75 - 1.0	1.0 - 1.5	1.5 - 2.0	2.0 - 2.5	2.5 - 3.5	3.5 - 4
0 - 0.25	0.1356	0.9767	-0.1924	-0.0664	-0.0140	-0.0009	-0.0001	-0.0000	0.0000
0.25 - 0.5	0.9767	0.4979	0.0279	-0.0191	-0.0128	-0.0031	-0.0007	-0.0001	-0.0000
0.5 - 0.75	-0.1924	0.0279	0.1102	0.0496	0.0026	-0.0041	-0.0017	-0.0004	-0.0001
0.75 - 1.0	-0.0664	-0.0191	0.0496	0.0920	0.0353	0.0005	-0.0029	-0.0011	-0.0003
1.0 - 1.5	-0.0140	-0.0128	0.0026	0.0353	0.0603	0.0174	0.0016	-0.0011	-0.0008
1.5 - 2.0	-0.0009	-0.0031	-0.0041	0.0005	0.0174	0.0372	0.0174	0.0025	-0.0007
2.0 - 2.5	-0.0001	-0.0007	-0.0017	-0.0029	0.0016	0.0174	0.0225	0.0076	0.0013
2.5 - 3.5	-0.0000	-0.0001	-0.0004	-0.0011	-0.0011	0.0025	0.0076	0.0088	0.0037
3.5 - 4	0.0000	-0.0000	-0.0001	-0.0003	-0.0008	-0.0007	0.0013	0.0037	0.0037

TABLE VII: Neutrino $d\sigma/dE_\pi$ statistical covariance matrix $\times 10^{-79}$. Note that the full uncertainty of the result is obtained by adding this covariance matrix to those in Tables VIII and IX.

$E_\pi(GeV)$	0 - 0.25	0.25 - 0.5	0.5 - 0.75	0.75 - 1.0	1.0 - 1.5	1.5 - 2.0	2.0 - 2.5	2.5 - 3.5	3.5 - 4
0 - 0.25	0.0469	0.2898	0.1137	0.1111	0.0805	0.0392	0.0194	0.0092	0.0046
0.25 - 0.5	0.2898	1.7901	0.7017	0.6859	0.4970	0.2426	0.1203	0.0570	0.0283
0.5 - 0.75	0.1137	0.7017	0.2757	0.2696	0.1950	0.0946	0.0466	0.0221	0.0111
0.75 - 1.0	0.1111	0.6859	0.2696	0.2636	0.1907	0.0925	0.0455	0.0216	0.0108
1.0 - 1.5	0.0805	0.4970	0.1950	0.1907	0.1381	0.0673	0.0333	0.0158	0.0079
1.5 - 2.0	0.0392	0.2426	0.0946	0.0925	0.0673	0.0334	0.0169	0.0080	0.0039
2.0 - 2.5	0.0194	0.1203	0.0466	0.0455	0.0333	0.0169	0.0086	0.0041	0.0020
2.5 - 3.5	0.0092	0.0570	0.0221	0.0216	0.0158	0.0080	0.0041	0.0019	0.0009
3.5 - 4	0.0046	0.0283	0.0111	0.0108	0.0079	0.0039	0.0020	0.0009	0.0005

TABLE VIII: Neutrino $d\sigma/dE_\pi$ flux systematic covariance matrix $\times 10^{-79}$

$E_\pi(GeV)$	0 - 0.25	0.25 - 0.5	0.5 - 0.75	0.75 - 1.0	1.0 - 1.5	1.5 - 2.0	2.0 - 2.5	2.5 - 3.5	3.5 - 4
0 - 0.25	0.7835	0.1193	0.0369	0.0302	0.0170	0.0085	0.0056	0.0029	0.0012
0.25 - 0.5	0.1193	1.4417	0.2816	0.1973	0.0913	0.0386	0.0276	0.0152	0.0064
0.5 - 0.75	0.0369	0.2816	0.2735	0.1186	0.0631	0.0243	0.0129	0.0062	0.0030
0.75 - 1.0	0.0302	0.1973	0.1186	0.2271	0.0666	0.0278	0.0142	0.0065	0.0031
1.0 - 1.5	0.0170	0.0913	0.0631	0.0666	0.1210	0.0205	0.0107	0.0047	0.0021
1.5 - 2.0	0.0085	0.0386	0.0243	0.0278	0.0205	0.0550	0.0068	0.0030	0.0012
2.0 - 2.5	0.0056	0.0276	0.0129	0.0142	0.0107	0.0068	0.0277	0.0021	0.0008
2.5 - 3.5	0.0029	0.0152	0.0062	0.0065	0.0047	0.0030	0.0021	0.0100	0.0005
3.5 - 4	0.0012	0.0064	0.0030	0.0031	0.0021	0.0012	0.0008	0.0005	0.0037

TABLE IX: Neutrino $d\sigma/dE_\pi$ non-flux systematic covariance matrix $\times 10^{-79}$

$E_\pi(GeV)$	0 - 0.25	0.25 - 0.5	0.5 - 0.75	0.75 - 1.0	1.0 - 1.5	1.5 - 2.0	2.0 - 2.5	2.5 - 3.5	3.5 - 4
0 - 0.25	0.2141	0.5504	-0.1078	-0.0621	-0.0139	-0.0004	0.0001	0.0001	-0.0000
0.25 - 0.5	0.5504	0.9801	0.1167	-0.0276	-0.0291	-0.0081	-0.0018	-0.0003	-0.0001
0.5 - 0.75	-0.1078	0.1167	0.2017	0.1025	0.0074	-0.0087	-0.0034	-0.0008	-0.0001
0.75 - 1.0	-0.0621	-0.0276	0.1025	0.1607	0.0591	0.0004	-0.0052	-0.0021	-0.0005
1.0 - 1.5	-0.0139	-0.0291	0.0074	0.0591	0.0875	0.0295	0.0034	-0.0016	-0.0010
1.5 - 2.0	-0.0004	-0.0081	-0.0087	0.0004	0.0295	0.0535	0.0241	0.0040	-0.0005
2.0 - 2.5	0.0001	-0.0018	-0.0034	-0.0052	0.0034	0.0241	0.0345	0.0125	0.0018
2.5 - 3.5	0.0001	-0.0003	-0.0008	-0.0021	-0.0016	0.0040	0.0125	0.0126	0.0047
3.5 - 4	-0.0000	-0.0001	-0.0001	-0.0005	-0.0010	-0.0005	0.0018	0.0047	0.0028

TABLE X: Anti-neutrino $d\sigma/dE_\pi$ statistical covariance matrix $\times 10^{-79}$. Note that the full uncertainty of the result is obtained by adding this covariance matrix to those in Tables XI and XII.

$E_\pi(GeV)$	0 - 0.25	0.25 - 0.5	0.5 - 0.75	0.75 - 1.0	1.0 - 1.5	1.5 - 2.0	2.0 - 2.5	2.5 - 3.5	3.5 - 4
0 - 0.25	0.0420	0.1947	0.1071	0.1179	0.0825	0.0341	0.0122	0.0019	0.0012
0.25 - 0.5	0.1947	0.9108	0.4947	0.5428	0.3779	0.1540	0.0537	0.0074	0.0049
0.5 - 0.75	0.1071	0.4947	0.2756	0.3041	0.2131	0.0886	0.0319	0.0052	0.0032
0.75 - 1.0	0.1179	0.5428	0.3041	0.3361	0.2360	0.0987	0.0358	0.0060	0.0036
1.0 - 1.5	0.0825	0.3779	0.2131	0.2360	0.1663	0.0703	0.0259	0.0046	0.0026
1.5 - 2.0	0.0341	0.1540	0.0886	0.0987	0.0703	0.0306	0.0118	0.0025	0.0013
2.0 - 2.5	0.0122	0.0537	0.0319	0.0358	0.0259	0.0118	0.0048	0.0012	0.0006
2.5 - 3.5	0.0019	0.0074	0.0052	0.0060	0.0046	0.0025	0.0012	0.0005	0.0002
3.5 - 4	0.0012	0.0049	0.0032	0.0036	0.0026	0.0013	0.0006	0.0002	0.0001

TABLE XI: Anti-neutrino $d\sigma/dE_\pi$ flux systematic covariance matrix $\times 10^{-79}$

$E_\pi(GeV)$	0 - 0.25	0.25 - 0.5	0.5 - 0.75	0.75 - 1.0	1.0 - 1.5	1.5 - 2.0	2.0 - 2.5	2.5 - 3.5	3.5 - 4
0 - 0.25	0.5242	0.6582	0.1663	0.0840	0.0262	0.0080	0.0058	0.0020	0.0002
0.25 - 0.5	0.6582	5.8193	1.0820	0.5440	0.1697	0.0509	0.0383	0.0153	0.0027
0.5 - 0.75	0.1663	1.0820	0.7139	0.2271	0.0783	0.0256	0.0199	0.0094	0.0026
0.75 - 1.0	0.0840	0.5440	0.2271	0.4017	0.0557	0.0196	0.0145	0.0070	0.0021
1.0 - 1.5	0.0262	0.1697	0.0783	0.0557	0.1649	0.0106	0.0072	0.0036	0.0012
1.5 - 2.0	0.0080	0.0509	0.0256	0.0196	0.0106	0.0903	0.0051	0.0025	0.0008
2.0 - 2.5	0.0058	0.0383	0.0199	0.0145	0.0072	0.0051	0.0505	0.0023	0.0007
2.5 - 3.5	0.0020	0.0153	0.0094	0.0070	0.0036	0.0025	0.0023	0.0195	0.0005
3.5 - 4	0.0002	0.0027	0.0026	0.0021	0.0012	0.0008	0.0007	0.0005	0.0041

TABLE XII: Anti-neutrino $d\sigma/dE_\pi$ non-flux systematic covariance matrix $\times 10^{-79}$

Degrees	0 - 5	5 - 10	10 -15	15 - 20	20 - 25	25 - 30	30 - 35	35 - 40	40 - 45	45 - 50	50 - 60	60 - 70
0 - 5	0.1518	0.0052	-0.0114	-0.0053	-0.0016	-0.0015	-0.0012	-0.0008	-0.0003	-0.0001	0.0000	0.0000
5 - 10	0.0052	0.1256	0.0078	-0.0083	-0.0031	-0.0012	-0.0005	-0.0003	-0.0004	-0.0001	-0.0000	-0.0000
10 -15	-0.0114	0.0078	0.0731	0.0085	-0.0045	-0.0018	-0.0009	-0.0004	-0.0002	-0.0001	-0.0000	-0.0000
15 - 20	-0.0053	-0.0083	0.0085	0.0569	0.0067	-0.0030	-0.0015	-0.0006	0.0002	-0.0001	-0.0001	-0.0000
20 - 25	-0.0016	-0.0031	-0.0045	0.0067	0.0374	0.0056	-0.0015	-0.0005	-0.0001	0.0002	-0.0000	-0.0000
25 - 30	-0.0015	-0.0012	-0.0018	-0.0030	0.0056	0.0289	0.0050	-0.0012	-0.0028	-0.0005	0.0000	0.0000
30 - 35	-0.0012	-0.0005	-0.0009	-0.0015	-0.0015	0.0050	0.0241	0.0054	-0.0023	-0.0024	-0.0004	0.0000
35 - 40	-0.0008	-0.0003	-0.0004	-0.0006	-0.0005	-0.0012	0.0054	0.0186	0.0072	-0.0007	-0.0011	-0.0002
40 - 45	-0.0003	-0.0004	-0.0002	0.0002	-0.0001	-0.0028	-0.0023	0.0072	0.0139	0.0058	-0.0005	-0.0005
45 - 50	-0.0001	-0.0001	-0.0001	-0.0001	0.0002	-0.0005	-0.0024	-0.0007	0.0058	0.0092	0.0024	-0.0001
50 - 60	0.0000	-0.0000	-0.0000	-0.0001	-0.0000	0.0000	-0.0004	-0.0011	-0.0005	0.0024	0.0057	0.0014
60 - 70	0.0000	-0.0000	-0.0000	-0.0000	-0.0000	0.0000	0.0000	-0.0002	-0.0005	-0.0001	0.0014	0.0053

TABLE XIII: Neutrino $d\sigma/d\theta_\pi$ statistical covariance matrix $\times 10^{-81}$. Note that the full uncertainty of the result is obtained by adding this covariance matrix to those in Tables XIV and XV.

Degrees	0 - 5	5 - 10	10 -15	15 - 20	20 - 25	25 - 30	30 - 35	35 - 40	40 - 45	45 - 50	50 - 60	60 - 70
0 - 5	0.0844	0.0923	0.0849	0.0911	0.0671	0.0540	0.0479	0.0365	0.0290	0.0150	0.0086	0.0016
5 - 10	0.0923	0.1013	0.0931	0.0998	0.0735	0.0592	0.0524	0.0400	0.0318	0.0165	0.0095	0.0018
10 -15	0.0849	0.0931	0.0856	0.0918	0.0676	0.0544	0.0482	0.0368	0.0292	0.0152	0.0087	0.0016
15 - 20	0.0911	0.0998	0.0918	0.0985	0.0725	0.0584	0.0517	0.0394	0.0313	0.0163	0.0093	0.0017
20 - 25	0.0671	0.0735	0.0676	0.0725	0.0534	0.0430	0.0381	0.0290	0.0231	0.0120	0.0069	0.0013
25 - 30	0.0540	0.0592	0.0544	0.0584	0.0430	0.0346	0.0307	0.0234	0.0186	0.0096	0.0055	0.0010
30 - 35	0.0479	0.0524	0.0482	0.0517	0.0381	0.0307	0.0272	0.0207	0.0165	0.0085	0.0049	0.0009
35 - 40	0.0365	0.0400	0.0368	0.0394	0.0290	0.0234	0.0207	0.0158	0.0126	0.0065	0.0038	0.0007
40 - 45	0.0290	0.0318	0.0292	0.0313	0.0231	0.0186	0.0165	0.0126	0.0100	0.0052	0.0030	0.0006
45 - 50	0.0150	0.0165	0.0152	0.0163	0.0120	0.0096	0.0085	0.0065	0.0052	0.0027	0.0016	0.0003
50 - 60	0.0086	0.0095	0.0087	0.0093	0.0069	0.0055	0.0049	0.0038	0.0030	0.0016	0.0009	0.0002
60 - 70	0.0016	0.0018	0.0016	0.0017	0.0013	0.0010	0.0009	0.0007	0.0006	0.0003	0.0002	0.0001

TABLE XIV: Neutrino $d\sigma/d\theta_\pi$ flux systematic covariance matrix $\times 10^{-81}$

Degrees	0 - 5	5 - 10	10 -15	15 - 20	20 - 25	25 - 30	30 - 35	35 - 40	40 - 45	45 - 50	50 - 60	60 - 70
0 - 5	0.1420	0.1742	0.1132	0.0416	0.0509	0.0353	0.0573	0.0565	0.0422	0.0258	0.0460	0.0530
5 - 10	0.1742	0.2246	0.1452	0.0569	0.0686	0.0492	0.0748	0.0740	0.0559	0.0351	0.0603	0.0682
10 -15	0.1132	0.1452	0.1047	0.0389	0.0476	0.0350	0.0532	0.0524	0.0399	0.0254	0.0420	0.0466
15 - 20	0.0416	0.0569	0.0389	0.0289	0.0235	0.0192	0.0218	0.0208	0.0157	0.0099	0.0147	0.0155
20 - 25	0.0509	0.0686	0.0476	0.0235	0.0380	0.0223	0.0277	0.0267	0.0204	0.0131	0.0194	0.0203
25 - 30	0.0353	0.0492	0.0350	0.0192	0.0223	0.0299	0.0218	0.0210	0.0163	0.0109	0.0149	0.0146
30 - 35	0.0573	0.0748	0.0532	0.0218	0.0277	0.0218	0.0433	0.0332	0.0261	0.0179	0.0262	0.0267
35 - 40	0.0565	0.0740	0.0524	0.0208	0.0267	0.0210	0.0332	0.0425	0.0265	0.0185	0.0271	0.0273
40 - 45	0.0422	0.0559	0.0399	0.0157	0.0204	0.0163	0.0261	0.0265	0.0279	0.0155	0.0224	0.0220
45 - 50	0.0258	0.0351	0.0254	0.0099	0.0131	0.0109	0.0179	0.0185	0.0155	0.0171	0.0167	0.0157
50 - 60	0.0460	0.0603	0.0420	0.0147	0.0194	0.0149	0.0262	0.0271	0.0224	0.0167	0.0298	0.0250
60 - 70	0.0530	0.0682	0.0466	0.0155	0.0203	0.0146	0.0267	0.0273	0.0220	0.0157	0.0250	0.0275

TABLE XV: Neutrino $d\sigma/d\theta_\pi$ non-flux systematic covariance matrix $\times 10^{-81}$

Degrees	0 - 5	5 - 10	10 -15	15 - 20	20 - 25	25 - 30	30 - 35	35 - 40	40 - 45	45 - 50	50 - 60	60 - 70
0 - 5	0.1863	0.0072	-0.0147	-0.0066	-0.0021	-0.0017	-0.0015	-0.0007	-0.0004	-0.0004	-0.0002	-0.0000
5 - 10	0.0072	0.2111	0.0400	0.0327	0.0796	0.0851	0.1135	0.0819	-0.0005	-0.0002	-0.0001	-0.0000
10 -15	-0.0147	0.0400	0.1386	0.0409	0.0420	0.0489	0.0665	0.0484	-0.0007	-0.0003	-0.0000	0.0000
15 - 20	-0.0066	0.0327	0.0409	0.1249	0.0720	0.0580	0.0802	0.0588	-0.0002	-0.0004	-0.0001	-0.0000
20 - 25	-0.0021	0.0796	0.0420	0.0720	0.1741	0.1116	0.1304	0.0950	0.0001	0.0003	-0.0001	-0.0001
25 - 30	-0.0017	0.0851	0.0489	0.0580	0.1116	0.1365	0.1258	0.0823	-0.0050	-0.0008	0.0000	0.0000
30 - 35	-0.0015	0.1135	0.0665	0.0802	0.1304	0.1258	0.1785	0.1090	-0.0053	-0.0047	-0.0006	0.0001
35 - 40	-0.0007	0.0819	0.0484	0.0588	0.0950	0.0823	0.1090	0.1135	0.0152	-0.0014	-0.0024	-0.0004
40 - 45	-0.0004	-0.0005	-0.0007	-0.0002	0.0001	-0.0050	-0.0053	0.0152	0.0314	0.0137	-0.0018	-0.0013
45 - 50	-0.0004	-0.0002	-0.0003	-0.0004	0.0003	-0.0008	-0.0047	-0.0014	0.0137	0.0198	0.0042	-0.0005
50 - 60	-0.0002	-0.0001	-0.0000	-0.0001	-0.0001	0.0000	-0.0006	-0.0024	-0.0018	0.0042	0.0123	0.0028
60 - 7	-0.0000	-0.0000	0.0000	-0.0000	-0.0001	0.0000	0.0001	-0.0004	-0.0013	-0.0005	0.0028	0.0119

TABLE XVI: Anti-neutrino $d\sigma/d\theta_\pi$ statistical covariance matrix $\times 10^{-81}$. Note that the full uncertainty of the result is obtained by adding this covariance matrix to those in Tables XVII and XVIII.

Degrees	0 - 5	5 - 10	10 -15	15 - 20	20 - 25	25 - 30	30 - 35	35 - 40	40 - 45	45 - 50	50 - 60	60 - 70
0 - 5	0.0552	0.0801	0.0547	0.0661	0.0640	0.0369	0.0322	0.0227	0.0184	0.0014	-0.0006	0.0042
5 - 10	0.0801	0.1166	0.0797	0.0961	0.0932	0.0540	0.0470	0.0333	0.0269	0.0022	-0.0008	0.0061
10 -15	0.0547	0.0797	0.0547	0.0659	0.0641	0.0370	0.0323	0.0229	0.0187	0.0016	-0.0004	0.0043
15 - 20	0.0661	0.0961	0.0659	0.0796	0.0774	0.0446	0.0390	0.0277	0.0226	0.0019	-0.0005	0.0052
20 - 25	0.0640	0.0932	0.0641	0.0774	0.0760	0.0438	0.0385	0.0276	0.0228	0.0022	-0.0003	0.0052
25 - 30	0.0369	0.0540	0.0370	0.0446	0.0438	0.0255	0.0223	0.0160	0.0132	0.0013	-0.0001	0.0030
30 - 35	0.0322	0.0470	0.0323	0.0390	0.0385	0.0223	0.0196	0.0141	0.0117	0.0012	-0.0001	0.0027
35 - 40	0.0227	0.0333	0.0229	0.0277	0.0276	0.0160	0.0141	0.0102	0.0086	0.0010	0.0000	0.0019
40 - 45	0.0184	0.0269	0.0187	0.0226	0.0228	0.0132	0.0117	0.0086	0.0074	0.0009	0.0002	0.0017
45 - 50	0.0014	0.0022	0.0016	0.0019	0.0022	0.0013	0.0012	0.0010	0.0009	0.0002	0.0001	0.0002
50 - 60	-0.0006	-0.0008	-0.0004	-0.0005	-0.0003	-0.0001	-0.0001	0.0000	0.0002	0.0001	0.0001	0.0001
60 - 70	0.0042	0.0061	0.0043	0.0052	0.0052	0.0030	0.0027	0.0019	0.0017	0.0002	0.0001	0.0004

TABLE XVII: Anti-neutrino $d\sigma/d\theta_\pi$ flux systematic covariance matrix $\times 10^{-81}$

Degrees	0 - 5	5 - 10	10 -15	15 - 20	20 - 25	25 - 30	30 - 35	35 - 40	40 - 45	45 - 50	50 - 60	60 - 70
0 - 5	0.0931	0.0923	0.0859	0.0256	0.0682	0.0426	0.0683	0.0556	0.0543	0.0173	0.0259	0.0859
5 - 10	0.0923	0.1068	0.0968	0.0311	0.0804	0.0525	0.0815	0.0675	0.0671	0.0246	0.0319	0.0988
10 -15	0.0859	0.0968	0.1070	0.0336	0.0804	0.0567	0.0837	0.0692	0.0696	0.0300	0.0353	0.0917
15 - 20	0.0256	0.0311	0.0336	0.0280	0.0347	0.0295	0.0354	0.0330	0.0334	0.0220	0.0182	0.0305
20 - 25	0.0682	0.0804	0.0804	0.0347	0.0848	0.0550	0.0756	0.0663	0.0659	0.0331	0.0341	0.0807
25 - 30	0.0426	0.0525	0.0567	0.0295	0.0550	0.0545	0.0566	0.0514	0.0519	0.0313	0.0280	0.0524
30 - 35	0.0683	0.0815	0.0837	0.0354	0.0756	0.0566	0.0856	0.0678	0.0682	0.0349	0.0352	0.0803
35 - 40	0.0556	0.0675	0.0692	0.0330	0.0663	0.0514	0.0678	0.0690	0.0612	0.0339	0.0321	0.0674
40 - 45	0.0543	0.0671	0.0696	0.0334	0.0659	0.0519	0.0682	0.0612	0.0693	0.0349	0.0326	0.0664
45 - 50	0.0173	0.0246	0.0300	0.0220	0.0331	0.0313	0.0349	0.0339	0.0349	0.0310	0.0197	0.0248
50 - 60	0.0259	0.0319	0.0353	0.0182	0.0341	0.0280	0.0352	0.0321	0.0326	0.0197	0.0216	0.0321
60 - 70	0.0859	0.0988	0.0917	0.0305	0.0807	0.0524	0.0803	0.0674	0.0664	0.0248	0.0321	0.1003

TABLE XVIII: Anti-neutrino $d\sigma/d\theta_\pi$ non-flux systematic covariance matrix $\times 10^{-81}$

$E_\nu(GeV)$	1.5 - 2.0	2.0 - 3.0	3.0 - 4.0	4.0 - 5.0	5.0 - 7.0	7.0 - 9.0	9.0 - 11.0	11.0 - 15.0	15.0 - 20.0
1.5 - 2.0	0.8354	-0.0235	-0.1095	-0.0082	-0.0004	0.0000	0.0000	-0.0000	-0.0000
2.0 - 3.0	-0.0235	0.0460	-0.0003	-0.0029	-0.0004	-0.0000	-0.0000	-0.0000	-0.0000
3.0 - 4.0	-0.1095	-0.0003	0.0334	0.0018	-0.0016	-0.0002	-0.0000	-0.0000	-0.0000
4.0 - 5.0	-0.0082	-0.0029	0.0018	0.0762	0.0054	-0.0029	-0.0004	-0.0001	-0.0000
5.0 - 7.0	-0.0004	-0.0004	-0.0016	0.0054	0.2284	0.0100	-0.0079	-0.0031	-0.0003
7.0 - 9.0	0.0000	-0.0000	-0.0002	-0.0029	0.0100	0.6263	0.0793	-0.0416	-0.0109
9.0 - 11.0	0.0000	-0.0000	-0.0000	-0.0004	-0.0079	0.0793	1.0676	0.2118	-0.0724
11.0 - 15.0	-0.0000	-0.0000	-0.0000	-0.0001	-0.0031	-0.0416	0.2118	1.2436	0.0420
15.0 - 20.0	-0.0000	-0.0000	-0.0000	-0.0000	-0.0003	-0.0109	-0.0724	0.0420	2.8417

TABLE XIX: Neutrino $\sigma(E_\nu)$ statistical covariance matrix $\times 10^{-78}$. Note that the full uncertainty of the result is obtained by adding this covariance matrix to those in Tables XX and XXI.

$E_\nu(GeV)$	1.5 - 2.0	2.0 - 3.0	3.0 - 4.0	4.0 - 5.0	5.0 - 7.0	7.0 - 9.0	9.0 - 11.0	11.0 - 15.0	15.0 - 20.0
1.5 - 2.0	0.1607	0.1059	0.0963	0.1011	0.2184	0.3017	0.3280	0.4243	0.6208
2.0 - 3.0	0.1059	0.0721	0.0614	0.0512	0.1267	0.1993	0.2206	0.2857	0.4143
3.0 - 4.0	0.0963	0.0614	0.0727	0.1065	0.1662	0.1811	0.1884	0.2465	0.3571
4.0 - 5.0	0.1011	0.0512	0.1065	0.2545	0.3247	0.1929	0.1667	0.2216	0.3363
5.0 - 7.0	0.2184	0.1267	0.1662	0.3247	0.5415	0.4320	0.4100	0.5299	0.7969
7.0 - 9.0	0.3017	0.1993	0.1811	0.1929	0.4320	0.5928	0.6354	0.8159	1.1904
9.0 - 11.0	0.3280	0.2206	0.1884	0.1667	0.4100	0.6354	0.6998	0.9011	1.3109
11.0 - 15.0	0.4243	0.2857	0.2465	0.2216	0.5299	0.8159	0.9011	1.1661	1.6954
15.0 - 20.0	0.6208	0.4143	0.3571	0.3363	0.7969	1.1904	1.3109	1.6954	2.4803

TABLE XX: Neutrino $\sigma(E_\nu)$ flux systematic covariance matrix $\times 10^{-78}$

$E_\nu(GeV)$	1.5 - 2.0	2.0 - 3.0	3.0 - 4.0	4.0 - 5.0	5.0 - 7.0	7.0 - 9.0	9.0 - 11.0	11.0 - 15.0	15.0 - 20.0
1.5 - 2.0	0.0454	0.0315	0.0316	0.0320	0.0366	0.0440	0.0506	0.0439	0.0410
2.0 - 3.0	0.0315	0.0401	0.0312	0.0320	0.0374	0.0444	0.0510	0.0469	0.0425
3.0 - 4.0	0.0316	0.0312	0.0489	0.0339	0.0404	0.0486	0.0566	0.0514	0.0448
4.0 - 5.0	0.0320	0.0320	0.0339	0.0577	0.0420	0.0503	0.0592	0.0545	0.0479
5.0 - 7.0	0.0366	0.0374	0.0404	0.0420	0.0961	0.0620	0.0735	0.0710	0.0627
7.0 - 9.0	0.0440	0.0444	0.0486	0.0503	0.0620	0.1203	0.0906	0.0830	0.0720
9.0 - 11.0	0.0506	0.0510	0.0566	0.0592	0.0735	0.0906	0.1689	0.1005	0.0847
11.0 - 15.0	0.0439	0.0469	0.0514	0.0545	0.0710	0.0830	0.1005	0.1551	0.0942
15.0 - 20.0	0.0410	0.0425	0.0448	0.0479	0.0627	0.0720	0.0847	0.0942	0.1494

TABLE XXI: Neutrino $\sigma(E_\nu)$ non-flux systematic covariance matrix $\times 10^{-78}$

$E_\nu(GeV)$	1.5 - 2.0	2.0 - 3.0	3.0 - 4.0	4.0 - 5.0	5.0 - 7.0	7.0 - 9.0	9.0 - 11.0	11.0 - 15.0	15.0 - 20.0
1.5 - 2.0	0.2440	0.0194	-0.0495	-0.0014	0.0044	-0.0004	-0.0000	-0.0000	0.0000
2.0 - 3.0	0.0194	0.0838	0.0015	-0.0059	-0.0009	-0.0000	0.0000	0.0000	-0.0000
3.0 - 4.0	-0.0495	0.0015	0.0590	0.0059	-0.0026	-0.0005	-0.0000	-0.0000	0.0000
4.0 - 5.0	-0.0014	-0.0059	0.0059	0.0967	0.0159	-0.0041	-0.0010	-0.0001	-0.0000
5.0 - 7.0	0.0044	-0.0009	-0.0026	0.0159	0.4430	0.0274	-0.0202	-0.0057	-0.0000
7.0 - 9.0	-0.0004	-0.0000	-0.0005	-0.0041	0.0274	1.6737	0.3357	-0.1557	-0.0181
9.0 - 11.0	-0.0000	0.0000	-0.0000	-0.0010	-0.0202	0.3357	3.4695	0.5463	-0.1972
11.0 - 15.0	-0.0000	0.0000	-0.0000	-0.0001	-0.0057	-0.1557	0.5463	5.0386	0.1996
15.0 - 20.0	0.0000	-0.0000	0.0000	-0.0000	-0.0000	-0.0181	-0.1972	0.1996	12.0922

TABLE XXII: Anti-neutrino $\sigma(E_\nu)$ statistical covariance matrix $\times 10^{-78}$. Note that the full uncertainty of the result is obtained by adding this covariance matrix to those in Tables XXIII and XXIV.

$E_\nu(GeV)$	1.5 - 2.0	2.0 - 3.0	3.0 - 4.0	4.0 - 5.0	5.0 - 7.0	7.0 - 9.0	9.0 - 11.0	11.0 - 15.0	15.0 - 20.0
1.5 - 2.0	0.0030	0.0131	0.0065	-0.0044	0.0083	0.0343	0.0521	0.0787	0.0342
2.0 - 3.0	0.0131	0.0761	0.0580	0.0073	0.0859	0.2405	0.3736	0.6081	0.3101
3.0 - 4.0	0.0065	0.0580	0.0721	0.0565	0.1320	0.2336	0.3659	0.6337	0.3403
4.0 - 5.0	-0.0044	0.0073	0.0565	0.1085	0.1740	0.1277	0.1769	0.3409	0.1411
5.0 - 7.0	0.0083	0.0859	0.1320	0.1740	0.4139	0.4506	0.6153	1.0507	0.4100
7.0 - 9.0	0.0343	0.2405	0.2336	0.1277	0.4506	0.9108	1.3782	2.2888	1.1480
9.0 - 11.0	0.0521	0.3736	0.3659	0.1769	0.6153	1.3782	2.1542	3.6281	1.9565
11.0 - 15.0	0.0787	0.6081	0.6337	0.3409	1.0507	2.2888	3.6281	6.2100	3.4856
15.0 - 20.0	0.0342	0.3101	0.3403	0.1411	0.4100	1.1480	1.9565	3.4856	2.3443

TABLE XXIII: Anti-neutrino $\sigma(E_\nu)$ flux systematic covariance matrix $\times 10^{-78}$

$E_\nu(GeV)$	1.5 - 2.0	2.0 - 3.0	3.0 - 4.0	4.0 - 5.0	5.0 - 7.0	7.0 - 9.0	9.0 - 11.0	11.0 - 15.0	15.0 - 20.0
1.5 - 2.0	0.0290	0.0236	0.0235	0.0204	0.0269	0.0299	0.0323	0.0330	0.0518
2.0 - 3.0	0.0236	0.1172	0.0995	0.0951	0.1161	0.1354	0.1505	0.1069	0.2238
3.0 - 4.0	0.0235	0.0995	0.1021	0.0900	0.1115	0.1298	0.1450	0.1098	0.2149
4.0 - 5.0	0.0204	0.0951	0.0900	0.1001	0.1077	0.1253	0.1438	0.1059	0.2070
5.0 - 7.0	0.0269	0.1161	0.1115	0.1077	0.1689	0.1719	0.1970	0.1474	0.2863
7.0 - 9.0	0.0299	0.1354	0.1298	0.1253	0.1719	0.2637	0.2278	0.1709	0.3551
9.0 - 11.0	0.0323	0.1505	0.1450	0.1438	0.1970	0.2278	0.4093	0.1736	0.3761
11.0 - 15.0	0.0330	0.1069	0.1098	0.1059	0.1474	0.1709	0.1736	0.2298	0.2809
15.0 - 20.0	0.0518	0.2238	0.2149	0.2070	0.2863	0.3551	0.3761	0.2809	0.7830

TABLE XXIV: Anti-neutrino $\sigma(E_\nu)$ non-flux systematic covariance matrix $\times 10^{-78}$